

Vegetation Image as Bayesian Predictor for Radio Propagation in Complex Environments Using Unscented Transform

Alexandre J. F. Loureiro¹, Leonardo R.A.X. Menezes¹, Glaucio L. Ramos², Paulo T. Pereira², Mateus H. B. Rezende²

¹ Dept. of Electrical Engineering, University of Brasilia, Brasilia/DF, Brazil, ² GAPEA - Antennas and Propagation Research Group, UFSJ, Ouro Branco/MG, Brazil

loureiro.alexandre@gmail.com, leonardo@ene.unb.br, glopesr@gmail.com, paulotiburciop@gmail.com, mateus.rezende@outlook.com

Abstract— Vegetation is considered a complex environment for analysis of scattering and attenuation in radio propagation phenomena. Satellite image processing can improve planning of radio systems with a vegetation attenuation predictor. In this research, the prediction is based on the correlation of more than 56% between RGB pixel values and vegetation attenuation taken from three groups of power measurements at two distinct regions of Brazil: Belo Horizonte, in the southeast region measured at 18 GHz, and Manaus at 24 GHz in the north region. The statistical analysis showed that more than 30% of the attenuation variance was due to the pixel values for each group. Using this linear correlated model between vegetation pixel RGB values and geolocated attenuation values, this work combined the unscented transform (UT) and Bayesian inference to refine the vegetation attenuation distribution. Since the necessary multiplication of Bayes prior and sampling distributions is not easily available in the UT, this paper presents a method that calculates new common sigma points and different new weights for the prior and sampling UT distributions, thus allowing the multiplication and creating the basis for a machine learning predictor tool.

Index Terms— Bayes Theorem, Centimeter Wave, Unscented Transform, Vegetation Propagation measurements.

I. INTRODUCTION

This work presents a simple procedure that helps the association of vegetation attenuation models with geographic information systems (GIS). Vegetation is intrinsic of most outdoor environments, and its main effects are modeled in the literature as a non-linear foliage attenuation component added to the free space path loss (FSPL) and a lower loss rate experienced due to the multiple contributions from different scatters [1]-[3]. While these models use vegetation depth penetration as main parameter, this research allows the addition of the vegetation image as another component to the models. The use of the vegetation image is based on the combination of the UT [4] and Bayes inference theorem [5]. This combination allows a continuous model fine tuning, when new measurement samples are available, thus creating the basis for a machine learning predictor tool

which can be applied to other knowledge areas.

Academia and industry are currently investigating the spectrums of cm-wave (3-30 GHz) and mm-wave (30-300 GHz) frequency bands to meet the 5G requirements [6][7]. The potential of cm-wave spectrum for commercial wireless access has attracting less research than mm-wave during the last years [8]. Some outdoor radio propagation characterization of 18 GHz, 24 GHz and other cmWave frequencies can be found in [6], [9] and [10].

Frequency is a key aspect in these models and compared with traditional cellular systems (below 6 GHz) the attenuation increases at cmWave/mmWave since smaller wavelengths fixed-size obstacles, such as a tree trunk or a leaf, cause higher blockage of the Fresnel clearance zone and scattering [11]. The vegetation increases the number of multipath components since at higher frequency bands a larger azimuth spreads are experienced due to the dominant contributions of the reflection and scattering mechanisms. The number of spatial multipath components in the suburban scenario with strong presence of vegetation is 1.23 times higher compared to the non-vegetated urban scenario [8].

The literature presents different vegetation attenuation models which can be classified as empirical, semi-empirical or analytical depending on the method to make the characterization of vegetation effects on propagation and the prediction of excess attenuation. The empirical models present simplest mathematical expressions and are easier to be applied but there is a strict dependence on specific measured data which determines the model parameters through regression curves fitted to the measured data. The physical process involved when the radio propagates through vegetation like scattering and absorption are not included in the empirical model [1]-[3]. Examples of empirical models are the Modified Exponential model (MED) [Weissberger, 1982], the ITU-R model [Stephens, 1998] and its Derivatives, the COST 235 [COST 235, 1996] and the Fitted ITU-R. The semi-empirical models present a best fit to measured data based on knowledge of the qualitative behavior of absorption and scatter in homogenous vegetation media. The geometry information of vegetation area is used at some sem-empirical models. Examples of semi-empirical models are the Non-Zero Gradient (NZG) model and the Dual Gradient (DG) model [1]. The analytical models use numerical analysis methods to provide solution for the physical processes involved in radio wave propagation through vegetation. Examples of analytical models are the Geometrical and Uniform Theory of Diffraction (GTD/UTD), the Radiative Energy Transfer Theory (RET), the Full Wave Solutions, and the Physical Optics [3]. These propagation models are needed for simulator tools used for wireless technology research and prediction tools used for radio network planning and optimization which use vegetation layers as input to calculate the propagation effects due foliage.

The lack of experimental studies specifically targeting foliage attenuation in the cm-wave frequency band can be solved using an alternative way to model this vegetation attenuation which is proposed in this article based on vegetation pixel RGB values extracted from digital satellite images as input to estimate the foliage attenuation. The methodology identified a correlation between vegetation pixel RGB values and vegetation measured attenuation values. The measured vegetation attenuation data

were supplied by the studies of a suburban tree clutter attenuation analysis with directional antennas at 18 GHz and 24 GHz cmWave radio propagation through vegetation which collected a set of dedicated directional measurements at two distinct vegetation scenarios of Brazil: Belo Horizonte, in the southeast region and Manaus, in the north region [8][10]. These previous studies presented a detailed analysis of spatial multipath components coming from the foliage including the tree clutter attenuation estimation based on the dedicated measurements.

A regression function was calculated to obtain the vegetation attenuation in dB as a function of the sum of RGB values from vegetation pixels in the propagation area. The propagation area considered is the intersection of the areas covered by the transmission antenna and reception antenna. Only the vegetation pixels inside the propagation areas were used and a filtering algorithm was applied. Some algorithms are available in the literature to filter vegetation cover from digital images which are widely used to describe vegetation quality and ecosystem changes and is a controlling factor in transpiration, photosynthesis and other terrestrial processes [12][13].

This article presents a method developed to use the Unscented Transform applied to the Bayes inference theorem. The Bayes inference theorem was used to calculate the posteriori expected vegetation attenuation for a prior RGB pixel distribution. The Unscented Transform, presented in the equation (1), applied to Bayes inference theorem was used to decrease the processing time to calculate the expected attenuation value and to decrease the number of vegetation pixel samples needed. Previous studies showed UT as an important method to decrease processing efforts and data samples needed [4], [14], [15].

$$E_d\{\hat{u}^k\} = \int_{-\infty}^{+\infty} \hat{u}^k \mathbf{w}(\hat{u}) d\hat{u} = \sum_i \mathbf{w}_i S_i^k \quad (1)$$

where,

- E_d is the expected value of the discrete distribution;
- \hat{u} represents the set of random variables, with probability distribution known;
- $\int_{-\infty}^{+\infty} \hat{u}^k \mathbf{w}(\hat{u}) d\hat{u}$ is the expected value E_c of the continuous distribution;
- S_i are the sigma points of UT;
- k is the order of approximation desired;
- w_i are defined as UT weights, in addition to be the discrete probability density function.

II. MEASUREMENT CAMPAIGN AND IMAGE PROCESSING

The measurement campaign was performed at two distinct vegetation scenarios. The first one was at 24 GHz centimeter wave (cmW) at Manaus, Amazonas, Brazil in a scenario with open spaces, scattered buildings and strong presence of vegetation (Fig. 1) [8]. The second scenario was at 18 GHz at Belo Horizonte, Minas Gerais, Brazil, in a university campus area, considered as suburban, with some buildings and considerable amount of vegetation (Fig. 2) [10]. At Manaus the average tree height is 9 meters and the canopies diameters range from 3 to 13 meters with estimated leaf size of 15

cm. A continuous-wave transmitter (TX) was placed at 15 meters height and the receiver (RX) used a rotating pedestal at 1.75 meters height, both sides with horn antennas of 25° half-power beam width (HPBW). A total of 12 foliage-obstructed TX-RX radio links were studied with distances ranging from 45 to 155 meters and direct TX-RX links through vegetation depth ranging from 3 to 15m. At each RX point the entire azimuth (0° to 360°) was swept by steps of 9° and for elevations of 10°, 20° and 30°. The continuous wave TX antenna at Belo Horizonte was mounted at 7 meters height and the RX used a rotating pedestal at 1.75 meters height, both sides with horn antennas with 16° of HPBW. At RX point 1 the entire azimuth (0° to 360°) was swept by steps of 10° and from -10 to +10 degrees in steps of 10 degrees in elevation. At the other RX points the antennas were aligned in respect to each other until the maximum field strength could be obtained. The vegetation attenuation was calculated for both scenarios as the average of received power for the various elevations minus FSPL and minus RX antennas gains. The measurement points (Fig. 1) at Manaus were separated in 2 groups: group 1 (1 up to 8) and group 2 (9 up to 12). These 2 groups will be applied to the method developed in this article which combines the UT technique with the Bayesian inference processes to refine the vegetation attenuation distribution. The Bayesian prior distribution will use group 1 and sampling distribution will use group 2.



Fig. 1. 3D View of vegetated scenario: TX and 12 measurement points at Manaus



Fig. 2. 3D View of vegetated scenario: TX and 5 measurement points at Belo Horizonte

The vegetation image processing was executed for both scenarios as follows:

- To capture satellite image was used a Google Earth API named “Google Static Maps API”. The date from satellite image from Manaus group 1 was 03/26/2015. The date from satellite image from Manaus group 2 was 10/13/2016. The date from satellite image from Belo Horizonte was 08/28/2017. This API was used to draw the propagation area considered is the intersection of the areas covered by the transmission antenna and reception antenna as presented at Fig. 3.
 - Exclude the buildings image pixels using the $L^*a^*b^*$ colorspace algorithm from Matlab image toolbox [12]. Filter vegetation pixels using this same algorithm. An example of the result is shown in the upper left of Fig. 3.
- Sum the RGB pixel values of vegetation at the polygon area formed by the points TX, RX and the intersection between TX and RX antennas (inside dash yellow polygon at Fig. 3). This was repeated for each azimuth by steps and for each measurement point.
- The sum of RGB pixels considered only the vegetation contiguous to the measurement point as the example shown at Fig. 3. The vegetation pixels considered were only those within the green rectangle area detailed in the upper left corner. Including non-contiguous vegetation pixels turned the correlation negative.
- Eliminate measurement points impacted by image watermark and eliminate links with azimuths impacted by building reflections.
- Normalization of pixel by area according the image size. The sum of RGB pixel values from Manaus group 2 image (Fig. 3) was multiplied by 3 since it has an area 3 times bigger than

the Manaus group 1 image which can be found at [16]. The sum of RGB pixel values from Belo Horizonte image (Fig. 4) was multiplied by 1.8 since it has an area 1.8 times bigger than the Manaus group 1 image which can be found at [16].

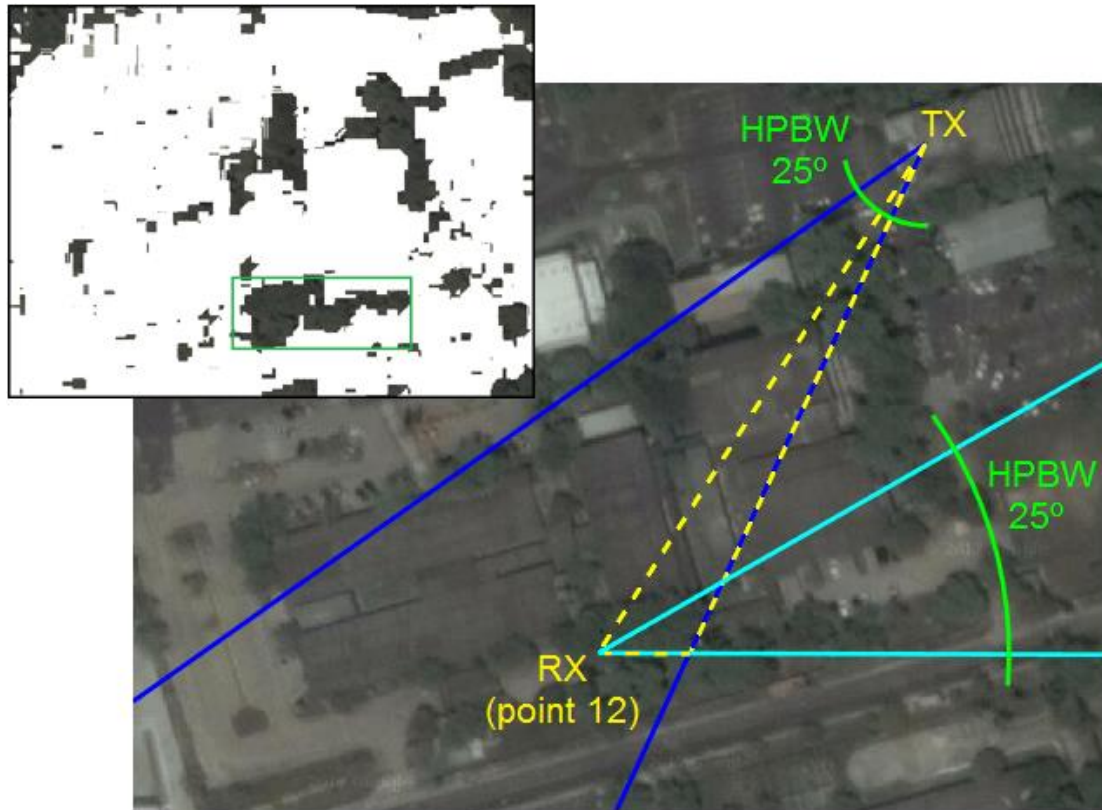


Fig. 3. Satellite image of group 2 at Manaus: yellow dashed area filtering vegetation pixels for point 12 and the upper left detail shows the green rectangle area filtering contiguous vegetation pixels for this same point



Fig. 4. 2D View of vegetated scenario: TX and 5 measurement points at Belo Horizonte

III. MAPPING RGB PIXELS TO ATTENUATION

A linear regression is obtained between vegetation attenuation and sum of RGB for each azimuth and point analyzed (Fig. 5 to Fig. 7). The correlation was 0.57 for Belo Horizonte, was 0.59 for Manaus group 1 and 0.56 for Manaus group 2. The regression showed that 32.4% of vegetation attenuation variation (R2 value) was due to the vegetation pixel values for Belo Horizonte, showed 34.8% for Manaus group 1 and 31.9% for Manaus group 2. The yellow marks at the figures 5 to 7 show the mean of attenuation and “sum of RGB pixels” for each point. The normalization of RGB sum was necessary to avoid numeric instability when calculating the UT distribution moments. The graphic at Fig. 6 differs from the one presented at [16] since a new method to filter vegetation pixels was used increasing the color and bright parameters from the satellite image.

The calculation of the UT attenuation distribution uses linear regression between the pixel distribution and the geolocated attenuation distribution, combined with the UT distribution of pixels (UT RGB).

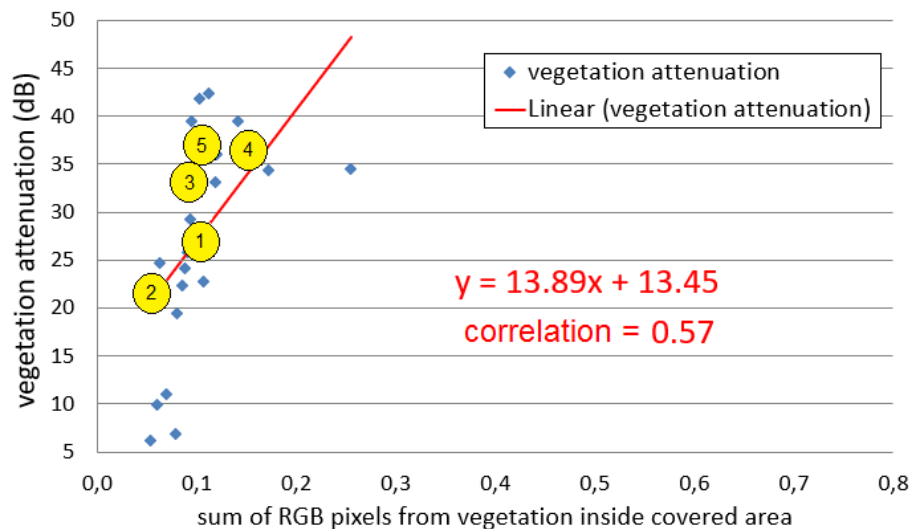


Fig. 5. Linear regression of vegetation attenuation measurements and pixel RGB values used to obtain the prior attenuation distribution at Belo Horizonte

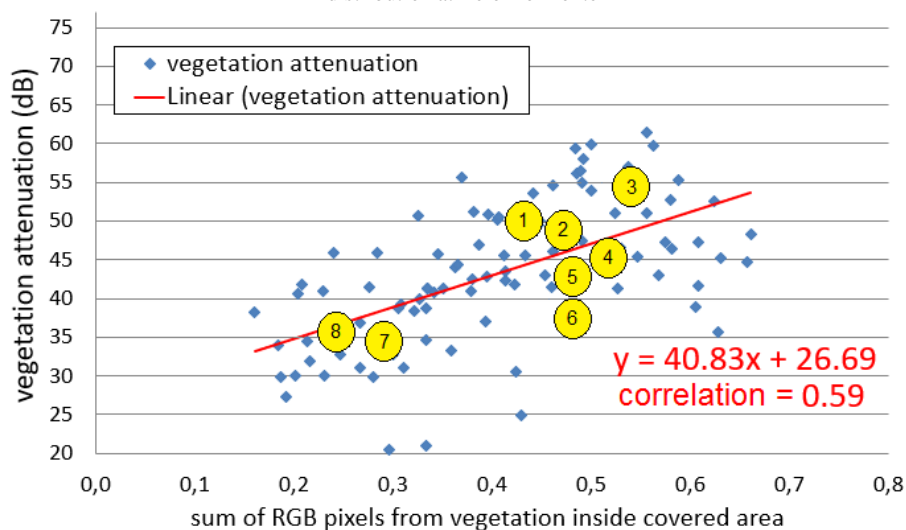


Fig. 6. Linear regression of vegetation attenuation measurements and pixel RGB values used to obtain the prior attenuation distribution at Manaus (group 1)

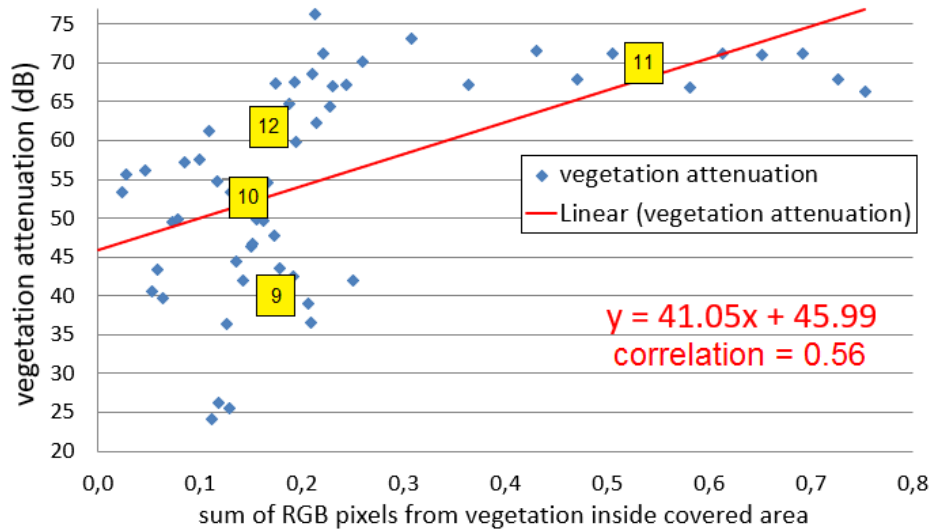


Fig. 7. Linear regression of vegetation attenuation measurements and pixel RGB values used to obtain the sampling attenuation distribution at Manaus (group 2)

These UT sigma points are mapped in the linear regression for the two measurement groups of Manaus (Fig. 6 and Fig. 7) to obtain the UT attenuation sigma points. These 2 groups applied to the method presented in the next section which combines the UT and Bayes will refine the vegetation attenuation distribution. The Bayesian UT prior distribution will use group 1 and the sampling UT distribution will use group 2. The weights of UT RGB and UT attenuation are the same. The figure 8 presents the six sigma points and weights calculated for the RGB and correlated attenuation distribution for group 1 and Fig. 9 presents the results for group 2. Figure 10 details the use of these UT distributions for groups 1 and 2 as prior and sampling distributions for Bayesian inference.

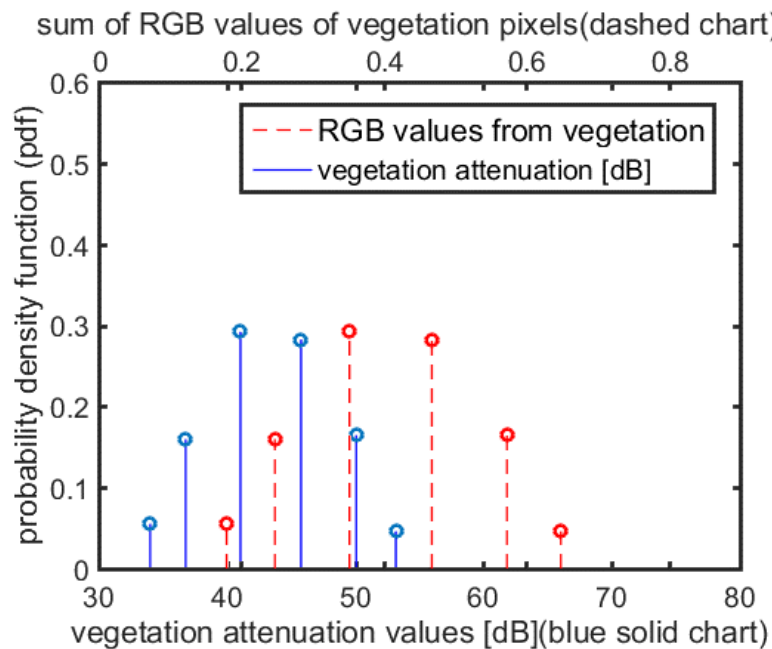


Fig. 8. UT distribution: vegetation attenuation and pixel values (group 1)

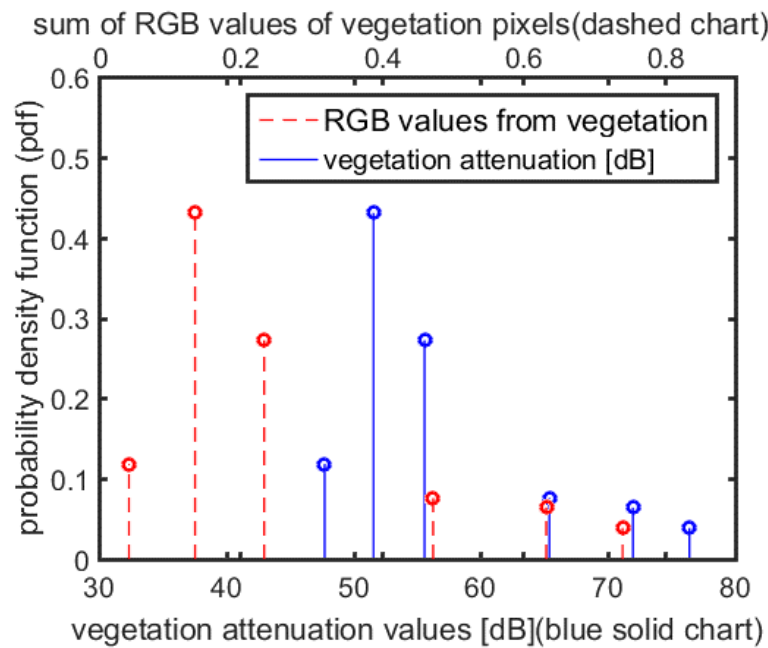


Fig. 9. UT distribution: vegetation attenuation and pixel values (group 2)

IV. COMBINING UT AND BAYES INFERENCE

Bayes' posteriori distribution $p(y|x)$ is obtained multiplying prior distribution $p(y)$ and sampling distribution $p(x|y)$ as (2), but the multiplication of UT distributions is not available in the state-of-the-art.

$$p(y | x) = \frac{p(x | y) \cdot p(y)}{\int_0^1 p(x | y) \cdot p(y) dy} \quad (2)$$

This work presents at Fig. 10, equation (3) and equation (4) a method to perform this calculation. The technique creates new prior and sampling UT distributions calculating new common sigma points (S_m), new weights for prior (p'_m) and new weights for sampling (p''_m). The new sigma points and weights of such distributions are calculated so that the statistical moments for prior $E\{\theta_1^k\}$ and sampling $E\{\theta_2^k\}$ are preserved. Equations (3) and (4) relates these new prior and sampling distributions with its previous sigma points (S_i and S_j) and weights (p_i and p_j).

$$\sum_{i=1}^N p_i S_i^k = \sum_{m=1}^N p'_m S_m^k = E\{\theta_1^k\} \quad (3)$$

$$\sum_{j=1}^N p_j S_j^k = \sum_{m=1}^N p''_m S_m^k = E\{\theta_2^k\} \quad (4)$$

Equation (2) can be calculated since common sigma points (S_m) are used in prior and sampling. The new prior and sampling distributions have different weights (p'_m and p''_m). θ_1 is the random variable for the prior distribution and θ_2 is the random variable for the sampling distribution.

The method presented at Fig. 10 and equations (3) and (4) was validated applying it to examples from [5] and one of these examples is presented as follow. Suppose a prior Beta distribution for a variable theta (θ) with mean 0.6 and standard deviation 0.3. Suppose a sampling Binomial distribution with $n=1000$ and $y=650$. The calculated Bayes posteriori distribution has a mean 0.6499 and a standard deviation 0.015.

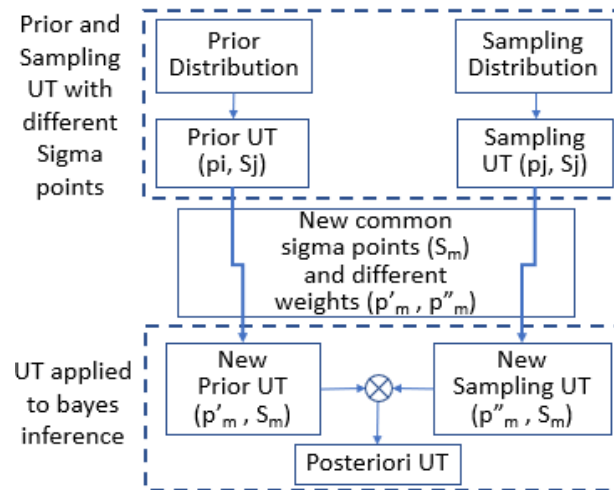


Fig. 10. Method developed to combine UT and Bayes inference

The UT with three sigma points and weights calculated for prior Beta distribution and sampling Binomial distribution are presented at Fig. 11. The calculation of Bayes UT posteriori distribution for this example is not possible since prior and sampling UT distributions does not have common sigma points and the multiplication needed at equation (2) will result zero.

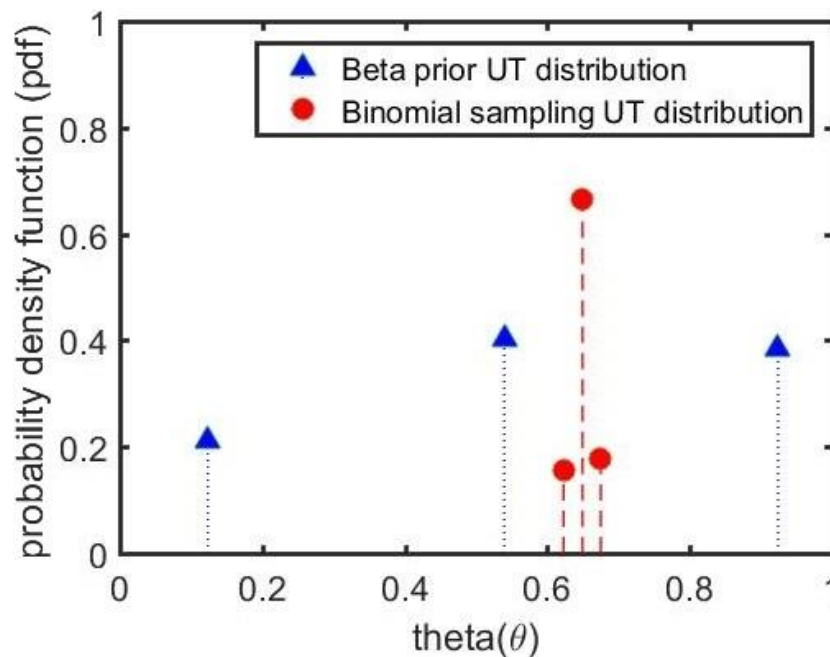


Fig. 11. Unscented Transform with three sigma points and weights for prior Beta distribution and sampling Binomial distribution without common sigma points

Applying the method from Fig. 10 is necessary to calculate three new common sigma points (S_m) for prior and sampling UT distributions, three new weights for prior (p'_m) and three new weights for sampling (p''_m). A group of nine equations are developed from equations (3) and (4) as presented at equations (5) to (13) below.

$$p'_{m1} S_{m1}^0 + p'_{m2} S_{m2}^0 + p'_{m3} S_{m3}^0 = E\{\theta_1^0\} = 1 \quad (5)$$

$$p'_{m1} S_{m1}^1 + p'_{m2} S_{m2}^1 + p'_{m3} S_{m3}^1 = E\{\theta_1^1\} = \text{mean}\{\theta_1\} \quad (6)$$

$$p'_{m1} S_{m1}^2 + p'_{m2} S_{m2}^2 + p'_{m3} S_{m3}^2 = E\{\theta_1^2\} \quad (7)$$

$$p'_{m1} S_{m1}^3 + p'_{m2} S_{m2}^3 + p'_{m3} S_{m3}^3 = E\{\theta_1^3\} \quad (8)$$

$$p''_{m1} S_{m1}^0 + p''_{m2} S_{m2}^0 + p''_{m3} S_{m3}^0 = E\{\theta_2^0\} = 1 \quad (9)$$

$$p''_{m1} S_{m1}^1 + p''_{m2} S_{m2}^1 + p''_{m3} S_{m3}^1 = E\{\theta_2^1\} = \text{mean}\{\theta_2\} \quad (10)$$

$$p''_{m1} S_{m1}^2 + p''_{m2} S_{m2}^2 + p''_{m3} S_{m3}^2 = E\{\theta_2^2\} \quad (11)$$

$$p''_{m1} S_{m1}^3 + p''_{m2} S_{m2}^3 + p''_{m3} S_{m3}^3 = E\{\theta_2^3\} \quad (12)$$

$$p''_{m1} S_{m1}^4 + p''_{m2} S_{m2}^4 + p''_{m3} S_{m3}^4 = E\{\theta_2^4\} \quad (13)$$

The solving of these nine equations calculates the prior and sampling UT distributions with three common sigma points (S_m) and new weights for prior (p'_m) and sampling (p''_m) as presented at the Fig. 12. These new prior and sampling UT distributions have the same moments (mean, variance, skewness) of previous distributions since this moments were used at the nine equations.

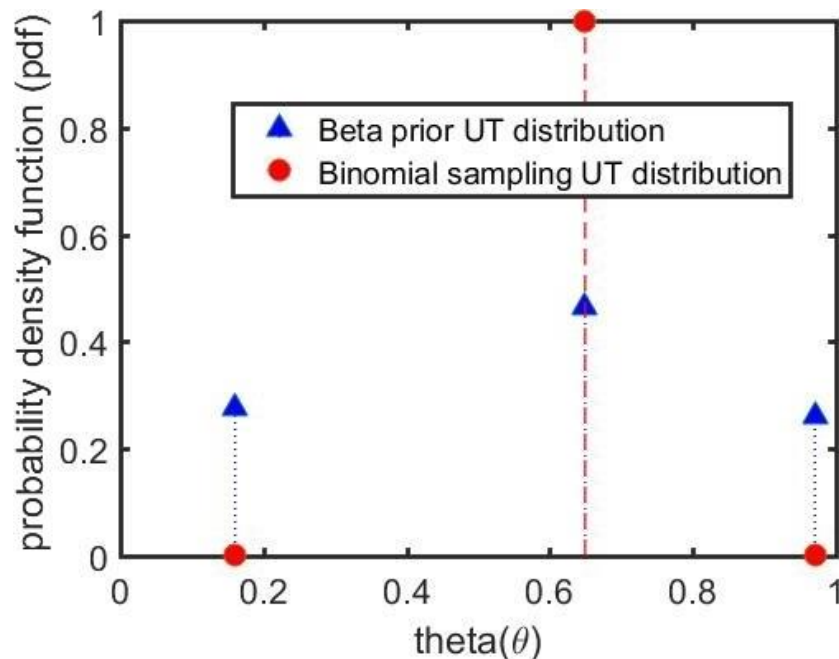


Fig. 12. Three UT common sigma points and different weights for prior Beta distribution and sampling Binomial distribution

The new prior UT Beta distribution for a variable θ keeps a calculated mean of 0.6 and the standard deviation 0.3. The new UT sampling Binomial distribution has mean 0.65 and the standard deviation 0.015. Since the new prior and sampling distributions have the same sigma points it is possible to multiply both distributions and calculate the UT posteriori Bayes distribution. The calculated UT posteriori Bayes distribution presented a mean 0.6496 and a standard deviation 0.011 which is closer to the mean 0.6499 and standard deviation 0.015 calculated at [5].

The number of equations needed to be developed from the equations (3) and (4) to calculate the common sigma points depends on how many sigma points are needed at the posteriori UT. Table 1 summarizes this analysis for some examples according to the number of posteriori UT sigma points needed.

TABLE I. NUMBER OF EQUATIONS AND MOMENTS NEEDED TO CALCULATE COMMON SIGMA POINTS

Posteriori Sigma Points (Sm)	New UT Prior weights (p'm)	New UT Sampling weights (p''m)	Number of Equations (Sm+ p'm + p''m)	Moments per Prior or Sampling distributions
2	2	2	6	3
3	3	3	9	5
4	4	4	12	6
5	5	5	15	8
n	n	n	3n	upper round (3n/2)

V. UT AND BAYES INFERENCE METHOD APPLIED TO VEGETATION ATTENUATION

The validated method was applied to calculate the posteriori UT vegetation attenuation distribution from prior and sampling UT distributions obtained from the power measurement campaign at Manaus and linear correlated RGB pixels values as presented at Fig. 13. New measurements can refine the posteriori distribution by generating new sampling UT attenuation distributions, since the prior attenuation will be backward fed by the posteriori as shown by red thick arrow at Fig. 13 thus creating the basis for a machine learning predictor tool.

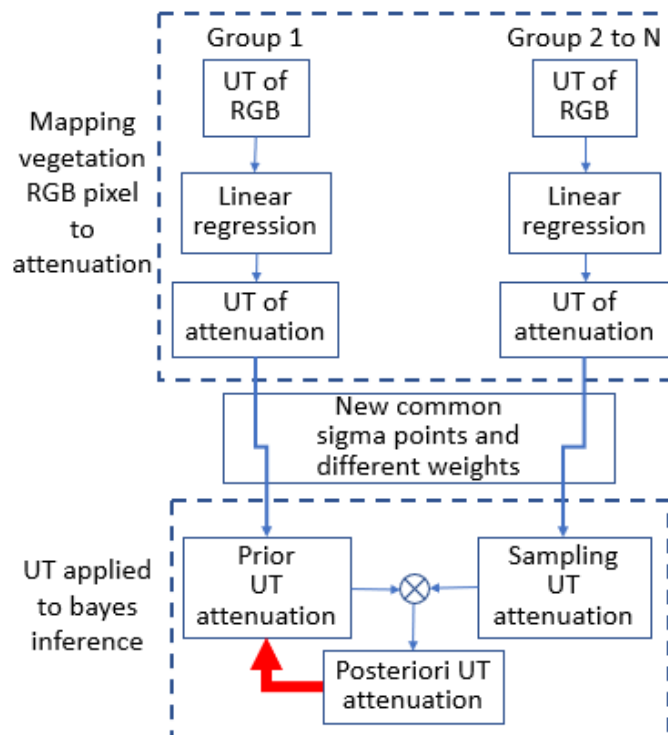


Fig. 13. Method mapping RGB pixel to attenuation and applying UT to Bayes inference getting the vegetation attenuation

Figure 14 shows the prior, sampling and posteriori UT distributions of vegetation attenuation. The posteriori UT attenuation with 6 sigma points was obtained from the multiplication of prior (group 1 of measurements) and sampling (group 2 of measurements). Different posteriori distributions were evaluated, with 6 or less UT sigma points, and the calculated expected attenuation varied only 1 dB.

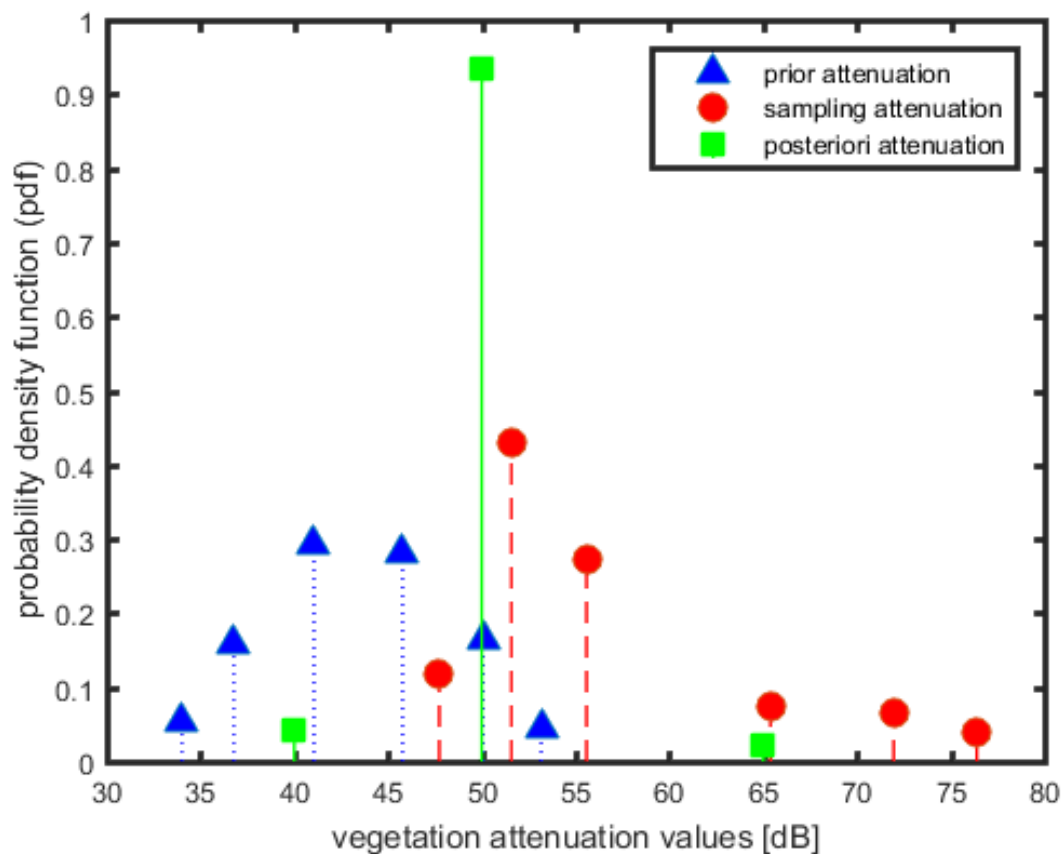


Fig. 14. UT distribution of vegetation attenuation for Manaus scenario: prior, sampling and posteriori

VI. CONCLUSION

This work presented a radio attenuation Bayesian predictor for vegetation based on image processing and the UT which was validated in two distinct vegetation scenarios. The image processing needs the elimination of buildings pixels, the filtering of vegetation pixels, the sum of vegetation pixels inside the antenna HPBW propagation area for each azimuth and the normalization of the sum of pixels by area according the image size.

Another key contribution is the compatibilization of the UT technique with Bayesian inference processes and this method was validated by a detailed example resolution. The combination of UT and Bayes inference can be applied in other areas like machine learning and artificial intelligence.

ACKNOWLEDGMENT

The authors would like to thank the Universidade de Brasília (UnB) and Electrical Engineering Department (ENE) for its support.

REFERENCES

- [1] J. Richter, R.F.S. Caldeirinha, Al-Nuaimi, et al., "A generic narrowband model for radiowave propagation through vegetation", *VTC IEEE*, Stockholm, Sweden, 2005, DOI: 10.1109/VETECS.2005.1543245
- [2] David. L. Jones et al., "Vegetation Loss Measurements at 9.6, 28.8, 57.6, and 96.1 GHz Through a Conifer Orchard in Washington State", *U.S. Department of Commerce*, NTIA Report 89-251, October 1989.
- [3] N.C. Rogers et al, "A generic model of 1-60 GHz radio propagation through vegetation-final report", Radio Comm. Agency, May 2002.

- [4] L.R.A.X. Menezes, A. Ajayi, C. Christopoulos, et al., "Efficient computation of stochastic electromagnetic problems using unscented transforms", *IET Science, Measurement & Technology*, 2008, 2, 2, p. 88-95, DOI: 10.1049/iet-smt:20070050
- [5] A. Gelman, J. B. Carlin, H. S. Stern, and D. B. Rubin, et al., "Bayesian Data Analysis", 3rd ed., Chapman and Hall Book, 2003. ISBN: 9781439898208
- [6] T. S. Rappaport et al., "Wideband Millimeter-Wave Propagation Measurements and Channel Models for Future Wireless Communication System Design", *IEEE Transactions on Comm.*, vol. 63, n° 9, Sep 2015.
- [7] P. Mogensen et al., "Centimeter-Wave Concept for 5G Ultra-Dense Small Cells", *IEEE Vehicular Technology Conference (VTC)*, May 2014.
- [8] I. Rodriguez et al., "24 GHz cmWave Radio Propagation Through Vegetation: Suburban Tree Clutter Attenuation", *European Conference on Antennas and Propagation (EuCAP)*, May 2016.
- [9] I. Rodriguez et al., "Analysis and Comparison of 24 GHz cmWave Radio Propagation in Urban and Suburban Scenarios", *IEEE Wireless Communications and Networking Conference*, April 2016.
- [10] M. H. B. Rezende, G. L. Ramos, et al., "18 GHz Propagation Measurements and Analysis in Belo Horizonte/Brazil", *IEEE-APS Topical Conference on Antennas and Propagation in Wireless Communications (APWC 2017)*, Verona, Italy, 2017, DOI: 10.1109/APWC.2017.8062251
- [11] T. S. Rappaport et al., "Millimeter Wave Wireless Communications", 1st Edition, *Prentice Hall*, 2015.
- [12] W. Song, X. Mu, G. Yan, S. Huang, "Extracting the Green Fractional Vegetation Cover from Digital Images Using a Shadow-Resistant Algorithm (SHAR-LABFVC)", *Remote Sensing*, 2015, 7, p. 10425-10443, DOI: 10.3390/rs70810425
- [13] Jiapaer, G.; Chen, X.; Bao, A. A comparison of methods for estimating fractional vegetation cover in arid regions. *Agric. Forest Meteorol.* 2011, 151, 1698–1710.
- [14] Fernandes, L.C., Menezes, L.R.A.X., "Using Unscented Transform in Interference Studies", *IEEE Antennas and Propagation Magazine*, 2017
- [15] S. J. Julier, J. K. Uhlmann, and H. F. Durrant-Whyte, "A new approach for filtering nonlinear systems", *Proc. Amer. Contr. Conf.*, pp. 1628-1632, 1995
- [16] L.R.A.X. Menezes, A.J.F. Loureiro, "cmWave through vegetation: correlation of pixels and attenuation using UT and Bayes Inference", *IEEE Antennas & Propagation Society Symposium. APSURSI*, San Diego, USA, 2017. DOI: 10.1109/APUSNCURSINRSM.2017.8072957